PLOS ONE

RESEARCH ARTICLE

Beyond greenness: Detecting temporal changes in photosynthetic capacity with hyperspectral reflectance data

Mallory L. Barnes[1]*, David D. Breshears[1,2], Darin J. Law[1], Willem J. D. van Leeuwen[1,3], Russell K. Monson[2], Alec C. Fojtik[4], Greg A. Barron-Gafford[3], David J. P. Moore[1]

1 School of Natural Resources and the Environment, University of Arizona, Tucson, Arizona, United States of America, **2** Department of Ecology and Evolutionary Biology, University of Arizona, Tucson, Arizona, United States of America, **3** School of Geography and Development, University of Arizona, Tucson, Arizona, United States of America, **4** Department of Geology, Wheaton College, Wheaton, Illinois, United States of America

* mallorybarnes@email.arizona.edu

Check for updates

OPEN ACCESS

Citation: Barnes ML, Breshears DD, Law DJ, van Leeuwen WJD, Monson RK, Fojtik AC, et al. (2017) Beyond greenness: Detecting temporal changes in photosynthetic capacity with hyperspectral reflectance data. PLoS ONE 12(12): e0189539. https://doi.org/10.1371/journal.pone.0189539

Editor: Krishna Prasad Vadrevu, University of Maryland at College Park, UNITED STATES

Received: June 16, 2017

Accepted: November 27, 2017

Published: December 27, 2017

Copyright: © 2017 Barnes et al. This is an open access article distributed under the terms of the Creative Commons Attribution License, which permits unrestricted use, distribution, and reproduction in any medium, provided the original author and source are credited.

Data Availability Statement: All relevant data are available from Open Science Framework at the following DOI: 10.17605/OSF.IO/ZUR8E.

Funding: This work was supported by the National Science Foundation Research Experience for Undergraduates: grant no. EAR-1263251 to ACF. The funder had no role in study design, data collection and analysis, decision to publish, or preparation of the manuscript.

Competing interests: The authors have declared that no competing interests exist.

Abstract

Earth's future carbon balance and regional carbon exchange dynamics are inextricably linked to plant photosynthesis. Spectral vegetation indices are widely used as proxies for vegetation greenness and to estimate state variables such as vegetation cover and leaf area index. However, the capacity of green leaves to take up carbon can change throughout the season. We quantify photosynthetic capacity as the maximum rate of RuBP carboxylation (V_{cmax}) and regeneration (J_{max}). V_{cmax} and J_{max} vary within-season due to interactions between ontogenetic processes and meteorological variables. Remote sensing-based estimation of V_{cmax} and J_{max} using leaf reflectance spectra is promising, but temporal variation in relationships between these key determinants of photosynthetic capacity, leaf reflectance spectra, and the models that link these variables has not been evaluated. To address this issue, we studied hybrid poplar (*Populus* spp.) during a 7-week mid-summer period to quantify seasonally-dynamic relationships between V_{cmax}, J_{max}, and leaf spectra. We compared *in situ* estimates of V_{cmax} and J_{max} from gas exchange measurements to estimates of V_{cmax} and J_{max} derived from partial least squares regression (PLSR) and fresh-leaf reflectance spectroscopy. PLSR models were robust despite dynamic temporal variation in V_{cmax} and J_{max} throughout the study period. Within-population variation in plant stress modestly reduced PLSR model predictive capacity. Hyperspectral vegetation indices were well-correlated to V_{cmax} and J_{max}, including the widely-used Normalized Difference Vegetation Index. Our results show that hyperspectral estimation of plant physiological traits using PLSR may be robust to temporal variation. Additionally, hyperspectral vegetation indices may be sufficient to detect temporal changes in photosynthetic capacity in contexts similar to those studied here. Overall, our results highlight the potential for hyperspectral remote sensing to estimate determinants of photosynthetic capacity during periods with dynamic temporal variations related to seasonality and plant stress, thereby improving estimates of plant productivity and characterization of the associated carbon budget.

Introduction

Photosynthesis by land plants plays a critical role in regional and global carbon balance [1–3]. Globally, photosynthesis in the terrestrial biosphere, combined with photosynthetic and non-photosynthetic processes in the oceans, offsets 45% of anthropogenic carbon emissions annually [4]. Terrestrial carbon uptake by plants varies annually and seasonally based on climate conditions [5–9], water and nutrient availability [10,11], and plant physiological properties such as water use efficiency [12] and photosynthetic capacity [13]. The size and future of the terrestrial carbon sink remains a critical uncertainty in global climate models [14]. To accurately predict terrestrial carbon uptake, improved quantification of spatial and temporal variation in photosynthesis is necessary.

Spatial and temporal variation in plant photosynthesis can be estimated using remote sensing-derived spectral indices. Spectral estimates of green vegetation, including vegetation indices such as the Normalized Difference Vegetation Index (NDVI), are widely used to estimate photosynthesis and vegetation productivity across spatial and temporal scales [15–18]. Estimates of gross primary productivity derived from greenness measures rely on relationships between vegetation use of light energy and photosynthesis [19–22]. However, the capacity of green leaves to use absorbed light to convert CO_2 into biomass varies dynamically throughout the season and with plant stress [23–26]. Many terrestrial biosphere models use static values of determinants of photosynthetic capacity [27]; however, there is some evidence that allowing photosynthetic capacity to vary temporally could improve representation of carbon dynamics [28]. The photochemical reflectance index (PRI) is a hyperspectral vegetation index that detects diurnal changes in xanthophyll cycle activity and responds to seasonal shifts in leaf pigment concentrations [29]. PRI is used to estimate photosynthetic light-use efficiency [30]; however, its relationship to photosynthetic capacity is unclear. Spectral methods that capture dynamic temporal changes in photosynthetic capacity could yield more accurate estimates of vegetation productivity and associated carbon uptake.

Photosynthetic capacity represents the potential of vegetation to fix CO_2 under optimal light and water conditions. In this study, we estimate photosynthetic capacity through measurements of the maximum rate of carboxylation of RuBP by the enzyme rubisco (V_{cmax}) and the maximum rate of electron transport driving RuBP regeneration (J_{max})[31]. Some terrestrial biosphere models treat V_{cmax} and J_{max} as fixed parameters [27]. However, these photosynthetic parameters vary in response to climate conditions [32–35], atmospheric CO_2 concentrations [36], plant stress [37], and seasonally in response to ontogenetic processes [38–40]. This seasonal variation can be important, given that process-based biosphere models that account for within-season variation in photosynthetic capacity show improved predictions of carbon flux dynamics [28].

Although hyperspectral remote sensing shows promise for predicting photosynthetic capacity based on leaf optical properties, questions remain regarding temporal variability. Estimates of photosynthetic capacity from remote sensing methods are desirable because of their potential to map V_{cmax} and J_{max} across space and constrain terrestrial biosphere model estimates of plant function. Predictive models of photosynthetic capacity, conditioned based on leaf reflectance metrics, have been developed using partial least squares regression (PLSR) for multiple tree species across glasshouse temperature regimes [29], in C4 crop species[41], and in C3 species at the canopy level [33]. Emergent studies on crop species using high-throughput phenotyping approaches further justify a better understanding of hyperspectral characterization of photosynthetic capacity [41–43]. Still unknown is whether hyperspectral methods of estimating V_{cmax} and J_{max} are robust to temporal variation in these key determinants of photosynthetic capacity. Hyperspectral leaf reflectance correlates with leaf characteristics likely to cause

seasonal variation in photosynthetic capacity such as chlorophyll content [44], nitrogen content [45], light-use efficiency [46], and water status [47], while spectral vegetation indices capture some but not all of these factors. However, previous studies have generally used variation in reflectance and plant function across space rather than time to derive these relationships so it remains unknown whether hyperspectral methods of estimating V_{cmax} and J_{max} are robust to temporal variation in these key determinants of photosynthetic capacity. We hypothesize that if seasonal variation in photosynthetic capacity is caused by a combination of leaf changes detectable by reflectance in bands outside of narrowband multispectral bands, then PLSR models that utilize the full reflectance spectrum will predict seasonal changes in V_{cmax} and J_{max}.

In this study, we evaluated the ability of hyperspectral data to represent and predict within-season temporal variation in V_{cmax} and J_{max} and examined the influence of water stress on the robustness of these estimates of photosynthetic capacity. We compared leaf reflectance spectra from hybrid poplar (*Populus* spp.*)* to V_{cmax} and J_{max} estimates throughout a 7-week period in the middle part of the growing season. We discuss our results in the context of emerging hyperspectral remote sensing methods and terrestrial biosphere models of global carbon dynamics.

Methods

Experimental site

Our study was conducted using poplar trees, grown outdoors at the Biosphere 2 Research Center near Oracle, AZ, USA (32˚ 34' 51" N 110˚ 50' 57" W; 1189 m). Biosphere 2 is leased to the University of Arizona. Authors RKM, DJPM, and GABG were responsible for the poplar stand at Biosphere 2. No additional permission was required to carry out this study, which did not involve endangered or protected species. We studied the relationship between spectral reflectance and photosynthetic capacity in 12 individual *Populus deltoides* hybrid poplar trees. Trees were planted in random arrangement with 1 x 1 m spacing in January 2013. Each year during the dormant season, the trees were coppiced and destructively sampled for biomass. Study trees were randomly selected before the start of the experiment in May 2016. During the study period (5/24/2016–7/5/2016), the mean high temperature was 34.4˚C and the mean low temperature was 21.3˚C. We applied 38 liters of water per day per tree during the pre-dawn period for 2 weeks prior to the start of the experiment (5/1/2016–5/14/2016) using an irrigation system to begin the study in well-watered conditions. We also fertilized the trees on 5/14/2016 using tree and shrub food (Arizona's Best) to ensure the trees were not nutrient-limited at the start of the induced dry-down. The trees were exposed to ambient climate conditions and had no irrigation except for supplemental watering from 6/2/2016 through 6/6/2016 and additional watering on 6/20/2016, which avoided senescence and caused variance in the water status of the trees. On sampling dates, we measured predawn leaf water potential (Ψ_{pd}), leaf gas exchange, and hyperspectral leaf reflectance for each tree. The full suite of measurements was conducted on all 12 trees on consecutive sampling dates (6 trees per day), except for 6/30 when we measured all 12 trees in one day.

Predawn leaf water potential and A/Ci curves

Predawn leaf water potential (Ψ_{pd}) was measured using a pressure chamber (PMS Instruments, Albany, OR, USA). Leaves were collected before sunrise, transported to the lab in a cooler, and measured within 30 minutes of collection. One leaf per plant was measured per time point.

Leaf gas exchange was measured with two LI-COR portable photosynthesis systems (LI-COR Biosciences, Lincoln, NE, USA) equipped with a 6400-02B LED light source. Gas

exchange measurements were performed on the youngest, most fully-expanded leaf on the south-facing side of each tree. Leaves were acclimated to the chamber at 25˚C, a chamber-air CO_2 concentration of 400 ppm, and a saturated photosynthetic photon flux density (PPFD) of 1800μmol m^{-2} s^{-1} until the photosynthetic rate (A) stabilized. Gas exchange curves were conducted only on leaves with an initial A $\geq$ 10 μmol CO_2 m^{-2} s^{-1} to ensure that the leaves were active enough to yield appropriate estimates for photosynthetic capacity. Each curve consisted of 13 different intercellular CO_2 concentrations (Ci) starting at the ambient CO_2 concentration of 400 ppm and then decreasing to 300, 200, 100, 50 to 0 ppm before increasing to 400, 400, 600, 800, 1200, 1600, 2000 ppm. We used the Predictive Ecosystem Analyzer (PEcAn) photosynthesis package to perform quality control of CO_2 response data before fitting A/Ci curves (https://github.com/PecanProject/pecan). In total, 86 CO_2 response curves passed quality control. We fit A/Ci curves using the 'fitaci' function in 'plantecophys' package in R [48]. The 'fitaci' function fits the Farquhar-Berry-Von Caemmerer Model of leaf photosynthesis [31] to measurements of photosynthesis and intercellular CO_2 and estimates V_{cmax} and J_{max} along with their standard errors.

Hyperspectral measurements

Reflectance was measured on the same leaves as the gas exchange measurements using a high-spectral resolution ASD FieldSpec® 3 Full-Range (350–2500 nm) spectroradiometer (Analytical Spectral Devices, Boulder, CO, USA). Reflectance measurements were taken with a leaf-clip assembly containing an internal calibrated light source and a black background panel face. The relative leaf reflectance data were standardized prior to measurements of each leaf by measuring a standard white reference reflectance target. ViewSpec Pro® software was used to convert binary data to ASCII data. The spectral resolution is 3nm at 700 nm, 10nm at 1400 and 2100nm across the full spectrum. The hyperspectral data are sampled at every 1nm. The spectroradiometer was turned on for at least 30 minutes before reflectance measurements were taken. The white panel reference reflectance was captured every 2–5 minutes. All measurements were taken from the leaf adaxial surface, avoiding the midrib. Three reflectance measurements were obtained on three different areas of each leaf lamina, resulting in nine spectra per leaf. Each measurement required no more than 5 s. Spectral reflectance measurements were quality-checked by removing negative reflectance values. We then averaged the nine spectra to determine mean optical properties for each leaf. Measures of leaf optical properties generally occurred between 10:30am and 11:30am and followed gas exchange measurements by no more than 2 hours.

Partial least squares regression models

Partial least-squares regression (PLSR) was performed to generate predictive models using the package 'PLS' in R [49]. PLSR is a multivariate regression method commonly used in spectroscopy because it can account for many related predictor variables and relatively few observations. PLSR identifies key components that explain variation in a trait variable and generates a linear model to transform full-spectrum data based on these components. The package 'PLSROpt' in R was used for pre-processing the spectral data in the order of standard normal variate, a second-derivative Savitzky-Golay smoother, auto-scaling, and mean centering (https://github.com/uwadaira/plsropt). The model with the number of components that minimized the Root Mean Squared Error of Prediction (RMSEP) was selected as the most parsimonious PLSR model. Each PLSR model was generated independently for V_{cmax} and for J_{max}. The spectrum range for all models was 450–2500 nm. Performance parameters were generated to assess the predictive ability of each model including the coefficient of determination (R^2).

Three different evaluations of the PLSR model were performed in increasing order of statistical rigor. The first test was a "leave-one-out" cross-validation approach, which trains the model on all but one observation, and then makes a prediction based on the single remaining observation [50]. The second test was performed with a 20% holdout dataset; a random 80/20% split of the data divided it into a training and testing dataset, respectively. New PLSR models were generated based on calibration of the training dataset and validated based on the remaining 20%. A 100x cross validation of training/calibration splits was performed to assess model and data stability across different proportions of testing and training data (S1 Fig). The third and most rigorous test of model stability was testing the model on the sampling dates with greatest variation in the population in terms of water stress (Ψ_{pd}). The two consecutive sampling dates with the largest individual variation in $\Psi_{pd,}$ (6/23/2016 and 6/24/2016, n = 12) were held out. The model was trained on all data except for the holdout dataset and was tested on the 12 observations with large variation in $\Psi_{pd.}$ The purpose of this test was to assess model predictive capacity in a situation with large within-population variation in environmental stress. For each PLSR model, Selectivity Ratio (SR) scores were calculated to enable comparison of the relative significance of each wavelength in its contribution to the final model. Although the Variable Importance of the Projection (VIP) score is more widely used in the current scientific literature, SR has been found to be more reliable for model predictions and is thus presented in this study [51].

Spectral vegetation indices

Spectral vegetation indices for estimating chlorophyll content, water stress, and carotenoid pigments were tested using the full set of observations (Table 1); these are all published indices used to estimate plant physiological status. The Normalized Difference Water Index (NDWI) was tested based on its correlation with plant water content in conifers [47], and PRI was tested based on known relationships with photosynthetic functioning [52,53] and environmental stress [54,55]. We also calculated 'MODIS-like' NDVI for all spectra. MODIS (Moderate Resolution Imaging Spectroradiometer) NDVI uses the red band (band 1; 620–670 nm) and the near-infrared (NIR) band (band 2; 841–876 nm). For both the red and NIR, we calculated the full-width- half-maximum for the subset of wavelengths corresponding to the MODIS bandwidths using the 'peakshape' function in the 'pavo' package [56]. We then took the mean of all reflectance values between the endpoints of the width of the spectrum curve. We then applied the standard NDVI equation (see Table 1) to get a 'MODIS-like' NDVI. Pairwise correlations between V_{cmax} and J_{max} estimated using standard gas exchange techniques and spectral indices were tested and R^2 reported.

Results

Weather conditions, photosynthetic capacity, and pre-dawn water potential (Ψ_{pd}) varied over the course of our study (Fig 1). Conditions were generally hot and dry throughout the study period, with high daytime temperatures and Vapor Pressure Deficit (VPD) and low precipitation (Fig 1A). Mean daytime temperature (06:00 to 18:00 MST) ranged from 20.73˚C to 38.90˚C throughout the study period with a mean of 30.1 ±4.3˚C. Peak VPD (10:00 to 14:00 MST) ranged from 0.60 kPa to 7.2 kPa with a mean of 3.9 ±1.3 kPa. There was little precipitation throughout the study period with most (30.3 mm) of the total rainfall (36.1 mm) occurring between 6-28-2016 and 6-30-2016 (Fig 1A). V_{cmax} and J_{max} both varied throughout the study period. V_{cmax} ranged from 43.9 to 130.4 with a mean of 75.7 ±20.8 μmol m^{-2} s^{-1}. J_{max} ranged from 76.7 to 261.2 with a mean of 150.1 ±37.5 μmol m^{-2} s^{-1}. V_{cmax} and J_{max} declined by approximately two-fold throughout the 7-week study period (Fig 1C and 1D). V_{cmax} and

Table 1. Hyperspectral vegetation indices that were compared to estimated V_{cmax} and J_{max} values.

Index	Formula	Reference	R^2 Vcmax	R^2 Jmax
SR1	ρ750/ρ700	Gitelson and Merzlyak 1997 [57]	**0.74**	**0.61**
Double Difference	(ρ749-ρ720)-(ρ701-ρ672)	le Maire et al. 2004 [58]	**0.74**	**0.58**
Vogelmann1	ρ740/ρ720	Vogelmann et al. 1993 [59]	**0.73**	**0.58**
mSR705	(ρ750-ρ445)/(ρ705-ρ445)	Sims and Gamon 2002 [44]	**0.73**	**0.57**
SRCarter	ρ760/ρ695	Carter et al. 1994 [60]	**0.72**	**0.61**
Maccioni	(ρ780-ρ710)/(ρ780-ρ680)	Maccioni et al. 2001 [61]	**0.72**	**0.55**
SR3	ρ750/ρ550	Gitelson and Merzlyak 1997 [57]	**0.70**	**0.63**
Gitelson	1/ρ700	Gitelson et al. 1999 [62]	**0.62**	**0.52**
NDVI (MODIS-like)	$(\rho NIR_{MODIS} - \rho Red_{MODIS})/(\rho NIR_{MODIS} + \rho Red_{MODIS})$	*see methods*	**0.60**	**0.50**
Datt4	ρ672/(ρ550*ρ708)	Datt (1998) [63]	**0.57**	0.45
SR4	ρ700/ρ670	McMurtey et al. (1994)	**0.57**	0.36
SR2	ρ752/ρ690	Gitelson and Merzlyak 1997 [42]	**0.56**	**0.53**
NDVI (hyperspectral)	(ρ860-ρ690)/(ρ860+ρ690)	Stimson et al. 2005 [47]	0.49	0.46
Vogelmann2	(ρ734-ρ747)-(ρ715+ρ726)	Vogelmann et al. 1993 [59]	0.17	0.14
mNDVI	(ρ800-ρ680)/(ρ800+ρ680–2ρ445)	Sims and Gamon 2002 [44]	0.07	0.03^{ns}
NDWI	(ρ860-ρ1240)/(ρ860+ρ1240)	Gao 1996 [64]	0.06	0.20
SIPI	(ρ800-ρ445)	Penuelas et al. 1995 [65]	0.06	0.03^{ns}
PRI	(ρ531-ρ570)/(ρ531+ρ570)	Gamon 1997 [52]	0.02^{ns}	0.00^{ns}
mSRCHL	(ρ800-ρ445)/(ρ680-ρ445)	Sims and Gamon 2002 [44]	0.00^{ns}	0.00^{ns}

The predictive formula (ρ = spectral reflectance) and reference for each index is shown in addition to the coefficient of determination for V_{cmax} and J_{max}. Nonsignificant correlations are indicated with an "ns" superscript. Values of R^2 above 0.50 are bolded.

https://doi.org/10.1371/journal.pone.0189539.t001

J_{max} appeared to stabilize following the rain events between 6-28-2016 and 6-30-2016 which relieved water stress (Fig 1B). Pre-dawn water potential varied seasonally, with the lowest water potentials (most stressed) generally occurring in the middle of the study period (6–23 and 6–24, Fig 1B). Water potential values ranged from -1.35 to -0.8 MPa with a mean of -0.45 ±0.23 MPa. Leaf reflectance varied between individuals and temporally (Fig 2A). We evaluated our results first in terms of variability in leaf reflectance spectra in the study period, then evaluated estimates of V_{cmax} and J_{max} from three different variations of PLSR models with increasing statistical rigor, and finally assessed relationships between V_{cmax} and J_{max} and published hyperspectral indices.

We performed three different evaluations of the PLSR models, presented in increasing order of statistical rigor. First, to assess the relationship between photosynthetic capacity and leaf spectra, PLSR models based on the complete dataset were developed. This least rigorous test of temporal stability used the "leave-one-out" cross validation approach to quantify the relationship between leaf reflectance spectra (450–2500 nm) and V_{cmax} and J_{max}. PLSR models predicted photosynthetic capacity accurately, with comparable model predictive ability for V_{cmax} (R^2 = 0.72; Fig 3A) and J_{max} (R^2 = 0.72; Fig 3B). The root mean squared error (RMSE) was lower for the V_{cmax} model (RMSE = 4.2, Fig 3A) than the J_{max} model (RMSE = 18.2, Fig 3B). The predictive model for V_{cmax} only required two components to explain the variance, while the PLSR model for J_{max} required four components.

Second, to assess temporal stability of the model, the data were split into training and testing datasets to generate PLSR models. This second test of PLSR model stability used 80% of the observations for training and withheld a 20% holdout dataset for testing. The 20% holdout dataset was randomly selected from the full dataset and the remaining 80% were used to build PLSR models for V_{cmax} and J_{max}. This procedure was performed 100 times with different

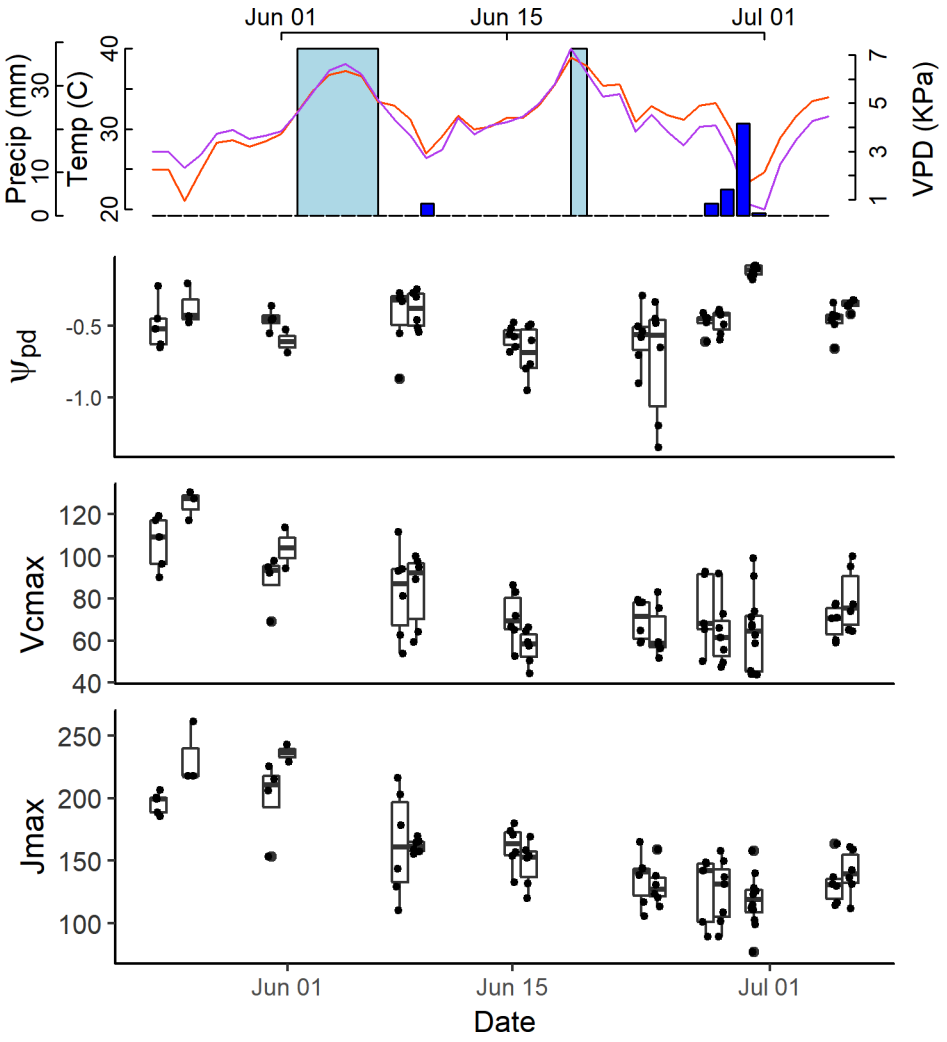

Fig 1. Temporal variability in meteorological and physiological conditions throughout the study period. A) shows mean daytime temperature in ˚C (orange line; 06:00 to 18:00), peak VPD in kPa (purple line; 10:00 to 14:00), precipitation in mm and supplemental watering throughout the study period with dark blue bars representing precipitation and light blue representing supplemental watering days. B) Shows the time series of predawn water potential (MPa) throughout the study period. C) and D) show the time series of estimated V_{cmax} (μmol m^{-2} s^{-1}) and J_{max} (μmol m^{-2} s^{-1}), respectively.

https://doi.org/10.1371/journal.pone.0189539.g001

randomly selected 20% holdout datasets (S1 Fig); the mean R^2 for the 80/20 split was 0.64 ±0.03 for V_{cmax} and 0.64 ±0.07 for J_{max} (S1 Table). Models with a 20% holdout dataset that were representative of mean predictive ability are shown in Fig 3C and 3D; predictive ability was comparable for V_{cmax} (R^2 = 0.67; Fig 3C) and J_{max} (R^2 = 0.69; Fig 3D). The predictive capability of the 80% model was similar to the predictive capability of the full cross-validated model (Fig 3A and 3B). The RMSE was lower for the V_{cmax} model (RMSE = 12.6; Fig 3C) than the J_{max} model (RMSE = 17.6; Fig 3D).

Third, to assess temporal stability in situations with large within-population variation in environmental stress, the data was split into a testing and training set based on variability in Ψ_{pd}. This third and most rigorous test of PLSR model stability trained the PLSR model on low environmental stress conditions (Ψ_{pd}) and tested it on the two consecutive sampling days with highest individual variation in $\Psi_{pd,}$ (6/23 and 6/24; Fig 1C). PLSR models for V_{cmax} and J_{max}

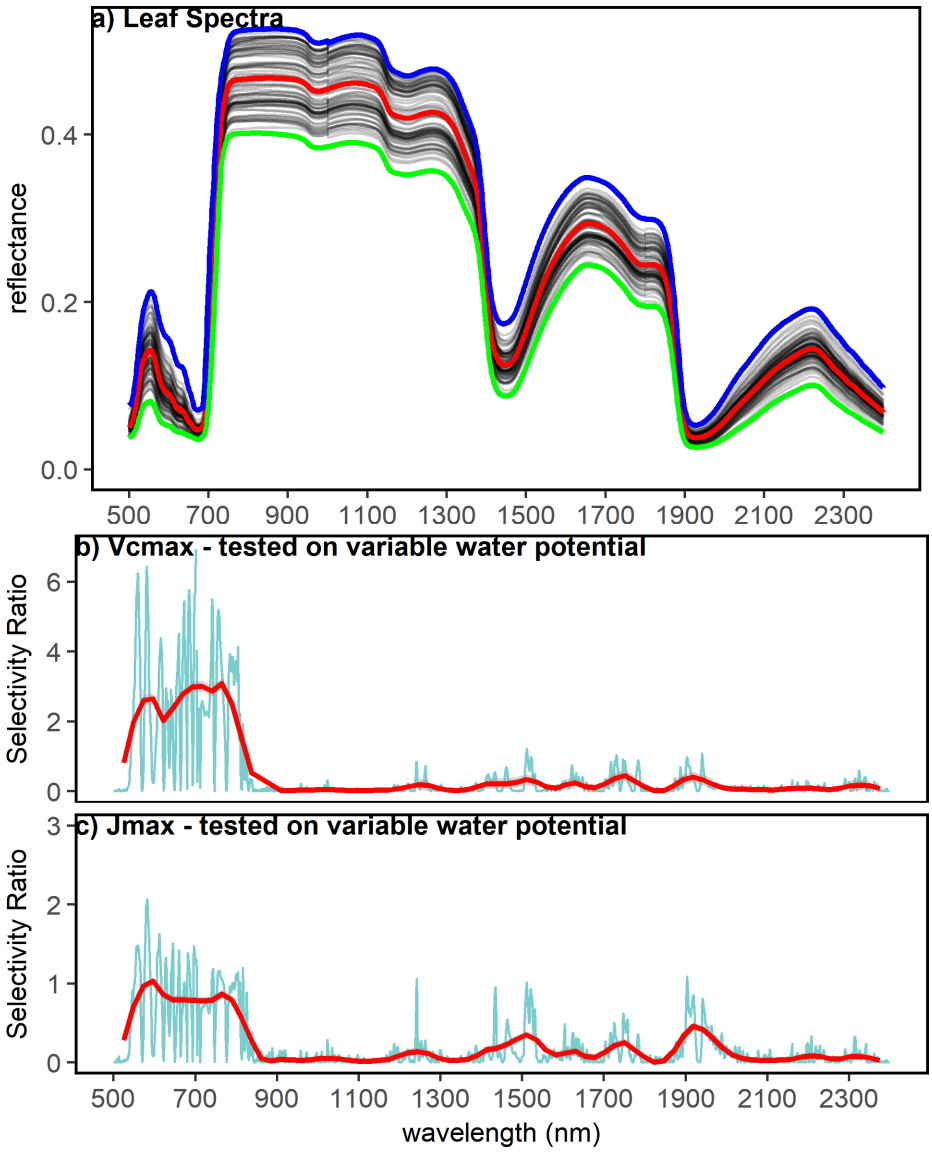

Fig 2. Leaf reflectance spectra and wavelength importance in PLSR models. (A) Pooled reflectance spectra (λ = 450–2500 nm) for all plants studied throughout the course of the study period (5/24/2016 to 7/05/2017). The mean reflectance at each wavelength is shown by the red line, the maximum and minimum reflectance at each wavelength are shown by the blue and green lines, respectively. (B)&(C): selectivity ratio of each wavelength in the PLSR models tested on variable water potential. (B) Shows the selectivity ratio of each wavelength in the V_{cmax} PLSR model, and (C) shows the selectivity ratio of each wavelength in the J_{max} PLSR model. The red lines in B&C are LOESS smoothers for visualization purposes.

https://doi.org/10.1371/journal.pone.0189539.g002

in this third test differed in their predictive abilities. The predictive ability was only moderately reduced for V_{cmax} (R^2 = 0.51; Fig 3E), whereas PLSR model predictive ability was substantially reduced for J_{max} (R^2 = 0.24; Fig 3F). The RSME was the same for both models (RMSE = 7.7; Fig 3E and 3F).

To compare the relative significance of different wavelengths in a given PLSR model, the selectivity ratio (SR) was used as a method of variable selection. The SR was used to assess relative contributions of different portions of the spectrum to the overall PLSR model. Both V_{cmax} and J_{max} models were sensitive to variation in the visible wavelength and near infrared (Fig 2B,

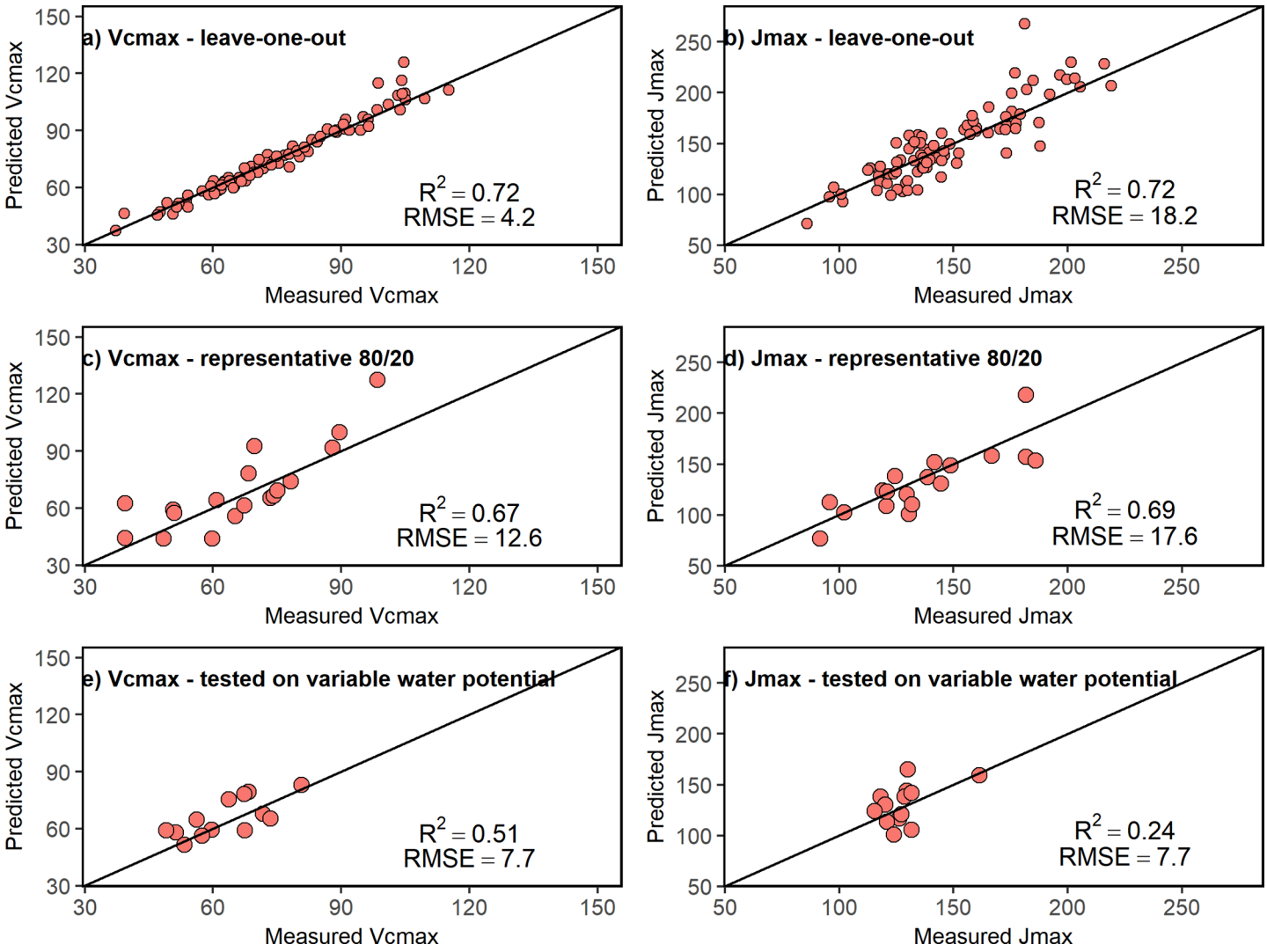

Fig 3. Temporal stability of PLSR models. All figures show observed vs. predicted values from PLS regression models. A&B: leave-one-out cross-validation procedure for (a) maximum rates of RuBP carboxylation (V_{cmax}, μmol m^{-2} s^{-1}) and (b) RuBP regeneration J_{max} (μmol m^{-2} s^{-1}), n = 86. C&D: representative 80/20% split of the data for PLSR (C) V_{cmax} (μmol m^{-2} s^{-1}) and (D) J_{max} (μmol m^{-2} s^{-1}). Each model was trained on 69 observations and tested on 17 observations. E & F: models tested on the period with the greatest between-individual variation in pre-dawn water potential (Ψ_{pd}) for (E) V_{cmax} (μmol m^{-2} s^{-1}) and (F) J_{max} (μmol m^{-2} s^{-1}). Each model was trained on 74 observations and tested on the 12 observations on 6/23/2016 and 6/24/2016 when the population varied widely in Ψ_{pd}. Statistical tests of increase in rigor moving downward.

https://doi.org/10.1371/journal.pone.0189539.g003

Fig 2C). Peak SR was at 703 nm for V_{cmax} and 583 nm for J_{max} (Fig 2B and 2C). Contributions from the short-wave infrared regions were small to both V_{cmax} and J_{max} models, however the SWIR contributed more to the J_{max} models than V_{cmax} models (Fig 2B and 2C).

To assess relationships between existing hyperspectral indices and photosynthetic capacity, correlations between V_{cmax} and J_{max} and a suite of hyperspectral vegetation indices were compared (Fig 4). Estimated V_{cmax} and J_{max} from hyperspectral chlorophyll and stress indices were well-correlated with measured values (Table 1). For V_{cmax}, four other metrics were all comparable to the full PLSR model (R^2 = 0.72) based on the coefficient of determination: Maccioni (R^2 = 0.72), Double Difference (R^2 = 0.74), Vogelmann2 (R^2 = 0.73), and SR1 (R^2 = 0.74) (Fig 4A). The PLSR model for J_{max} (R^2 = 0.72) outperformed all tested hyperspectral indices, the best of which was SR3 (R^2 = 0.63; Fig 4B). Several indices had very low or non-significant

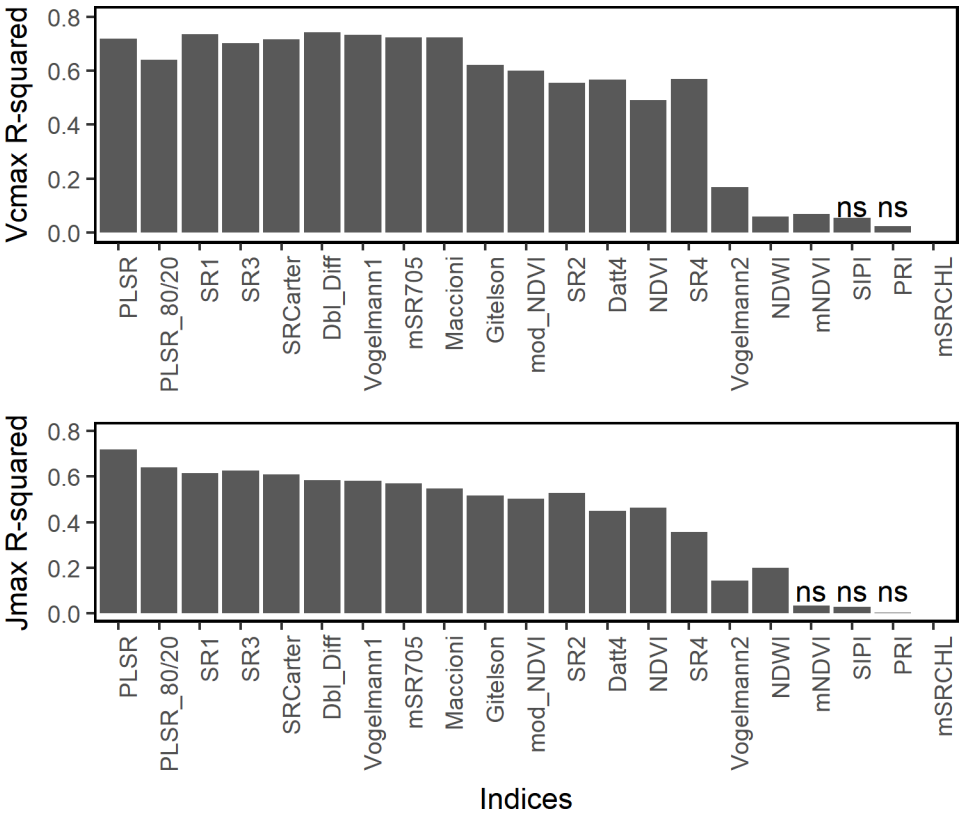

Fig 4. Comparison of predictive abilities of hyperspectral indices and PLSR models. Predictive capability for (A) maximum rates of RuBP carboxylation (V_{cmax}, μmol m^{-2} s^{-1}) and (B) RuBP regeneration J_{max} (μmol m^{-2} s^{-1}). Pairwise correlations between V_{cmax} and J_{max} estimated using standard gas exchange techniques and spectral indices were tested and R^2 is reported. The R^2 reported for the PLSR model is from the leave-one-out cross-validation approach. Indices with non-significant correlations are represented with "ns".

https://doi.org/10.1371/journal.pone.0189539.g004

correlations with V_{cmax}, including PRI, NDWI, mNDVI, and SIPI (Table 1). The mNDVI, SIPI, PRI, and mSRCHL indices all had non-significant relationships with Jmax (Table 1). The hyperspectral normalized difference vegetation index (NDVI) had moderate predictive capability for Vcmax (R^2 = 0.49) and J_{max} (R^2 = 0.46). The MODIS-like NDVI ("mod_NDVI") performed better than the hyperspectral NDVI for both V_{cmax} (R^2 = 0.60) and J_{max} (R^2 = 0.50) (Fig 4, Table 1).

Discussion

Our results show that hypers can predict photosynthetic parameters across time, suggesting that these hyperspectral remote sensing techniques have great potential to constrain model estimates of plant function. In this study, relationships between leaf reflectance spectra and photosynthetic capacity were robust throughout a 7-week period with dynamic change in photosynthetic capacity. Hyperspectral vegetation indices to estimate chlorophyll content were correlated with the key determinants of photosynthetic capacity, V_{cmax} and J_{max}. Predictions of V_{cmax} and J_{max} from PLSR models derived from leaf reflectance spectra were proportionally-sensitive to observed variation in V_{cmax} and J_{max}. These results support our hypothesis that PLSR models that utilize the full spectrum can predict photosynthetic capacity through time. These findings highlight the potential of hyperspectral remote sensing methods to

accurately predict V_{cmax} and J_{max} despite dynamic temporal variation in photosynthetic capacity related to within-season variation and plant stress.

Leaf-level hyperspectral data have previously been used to estimate photosynthesis [66] and photosynthetic capacity across temperature regimes in glasshouse experiments [32], and in diverse agroecosystems [41,42], but our study is the first to assess the impacts of *in situ* within-season temporal variation on estimates of photosynthetic capacity derived from leaf reflectance spectra. As in previous studies, measured and PLSR-modeled leaf traits were significantly correlated [32,42,66,67]. Regression models predicted V_{cmax} and J_{max} during a 7-week period with dynamic declines in photosynthetic capacity. This is confirmation that the spectral signals detected by leaf reflectance observations are accurately tracking seasonal metabolic adjustments made within the photosynthetic machinery of the leaf. When PLSR models were trained on only 80% of the data and tested on the remaining 20%, their mean predictive capability were similar to that of the full PLSR models. This shows that relationships between leaf reflectance spectra and V_{cmax} and J_{max} are robust despite large variation in these values. Known hyperspectral vegetation indices had varying predictive capabilities. Hyperspectral vegetation indices developed for estimating chlorophyll content (e.g. SR1, Double Difference, Vogelmann 1) and plant stress (SRCarter) had the highest correlations with plant photosynthetic capacity (Table 1). The wavelengths that explained variance in photosynthetic capacity in the PLSR models (based on selectivity ratio) were consistent with the wavelengths that comprised the best-performing hyperspectral indices. The important wavelengths in PLSR models, based on Selectivity Ratio, for predicting V_{cmax} and J_{max} largely fell in the visible and short wavelength end of the near-infrared (~500 to 850 nm), with minor contributions from wavelengths in the short-wave infrared. Important wavelengths in the visible region fell largely in the blue region (450–495 nm) and red regions (620–650 nm) for the V_{cmax} models, which is consistent with the chlorophyll absorption regions (i.e. ~430–460 nm and 640–670 nm). The highest-performing hyperspectral vegetation indices generally leveraged diagnostic differences in the red-edge portion (680–750 nm) of the spectrum to estimate chlorophyll content. The red edge region of reflectance is known to be sensitive to differences in chlorophyll content, and chlorophyll content is generally positively correlated with photosynthetic capacity [68]. Overall, both hyperspectral indices and PLSR models had the capability to predict variation in within-season photosynthetic capacity.

Accurate representation of photosynthesis in terrestrial biosphere models is essential to predicting future carbon and global change dynamics [69]. Although modeled rates of photosynthesis are sensitive to V_{cmax} and J_{max} [3,70,71], most terrestrial biosphere models use static values for these parameters [27]. Furthermore, V_{cmax} and J_{max} values are often parameterized based on limited or poorly represented data sets [27]. Monthly optimization of V_{cmax} improved process-based biosphere model (Organizing Carbon and Hydrology in Dynamic Ecosystems; ORCHIDEE) representation of seasonal carbon dynamics (NEE; Net Ecosystem Exchange) in a tropical evergreen forest in Brazil, however, seasonal parameter variations could not be extrapolated spatially [28]. Remote sensing observations can improve model representation of photosynthesis across spatial and temporal scales [31,55,72]. Our results support the use of remotely sensed estimation of photosynthetic capacity using hyperspectral observations. Furthermore, hyperspectral remote sensing could be used to incorporate spatially explicit photosynthetic capacity/environment relationships in next-generation trait-based models. Our results highlight the potential of hyperspectral remote sensing to parameterize determinants of photosynthetic capacity and inform trait-environment relationships in terrestrial biosphere models, thereby improving model representation of photosynthesis and carbon dynamics.

Although PLSR model predictive capabilities for V_{cmax} and J_{max} were generally similar, there were differences in PLSR model performance and sensitivity between the two variables. The mean predictive capability of the 80% PLSR models were comparable for V_{cmax} and J_{max}

(Table 1); however, the variance in J_{max} was nearly twice that of the variance in V_{cmax} (Table 1, S1 Fig). A rigorous test of PLSR model performance in the population with individual variation in drought stress indicated modest reductions in predictive capability for V_{cmax} and substantial reductions in predictive capability for J_{max}. This test of temporal stability indicates that predictive relationships between leaf reflectance spectra and photosynthetic capacity are reduced when there is within-population variation in environmental stress, particularly for J_{max}. PLSR models for J_{max} included more wavelengths in the short-wave infrared that are associated with leaf water content and internal structure. The performance improvement of the PLSR model for J_{max} compared to simple indices underscores the importance of full spectral information for predicting this parameter (Fig 4B)[42]. Terrestrial biosphere models generally simulate J_{max} as a function of V_{cmax} rather than as its own parameter [73]. However, our results suggest that V_{cmax} and J_{max} may be differentially sensitive to within-population variation in environmental stress.

Quantifying temporal variation in relationships between photosynthetic capacity and leaf reflectance spectra is timely given the increasing availability of high resolution spectral remote sensing, such as hyperspectral overflights planned by the National Ecological Observatory Network (NEON) [74] and NASA's Hyperspectral Infrared Imager (HyspIRI) mission [75]. NEON hyperspectral overflights, which may only occur once per year over a given region, may be used to develop predictive relationships between leaf reflectance spectra and photosynthetic capacity. Our results suggest that such predictive relationships developed from data in a short portion of the growing season could hold true throughout the growing season. The widely used NDVI had moderate predictive capacity for V_{cmax} and J_{max}. Notably, our approximation of MODIS NDVI had higher predictive capacity than hyperspectral NDVI (Table 1). Detecting temporal changes in photosynthetic capacity using MODIS NDVI could improve model predictions of photosynthesis given its broad spatial and daily temporal coverage. Another important consideration in extrapolating the results of this study to aerial and satellite remote sensing is additional technical challenges posed by these approaches, such as view angle effects, canopy architecture, and atmospheric effects. More studies are needed to further test temporal stability of relationships between leaf reflectance spectra and photosynthetic capacity in other contexts before relationships from a single hyperspectral overflight can be extrapolated through the growing season. Nonetheless, our results suggest promise for this approach.

In this study, spectral estimation of V_{cmax} and J_{max} in hybrid poplar was robust to temporal variation of up to 200% in photosynthetic capacity. Applying remote sensing tools to predict photosynthetic capacity across a wider range of wildlands requires an *in situ* test of this method outside of agroecosystem or controlled glasshouse conditions across a time period of variable abiotic and biotic conditions. Our results show that relationships between photosynthetic capacity and leaf reflectance spectra developed from limited data can in some cases be extrapolated temporally. These results highlight the potential of hyperspectral remote sensing methods to detect dynamic temporal variations in V_{cmax} and J_{max} related to seasonality and plant stress, thereby aiding improved estimates of plant productivity and associated carbon budget. Furthermore, our results suggest that terrestrial biosphere models could use hyperspectral remote sensing to parameterize V_{cmax} and J_{max} within season to improve predictions of future carbon dynamics. Reliable and precise methods to estimate V_{cmax} and J_{max} across spatial and temporal scales will improve understanding of ecosystem carbon uptake and the terrestrial carbon sink.

Supporting information

S1 Fig. Variance of R^2 values based on proportion of data used for training the PLSR model. Each point represents the r-squared between predicted and actual Vcmax/Jmax values

from PLSR using a random sample corresponding to the designated proportion of training data (each proportion was sampled 100 times).
(TIF)

S1 Table. Mean, median, and standard deviation of R^2 values based on proportion of data used for training the PLSR model. The mean, median, and standard deviation in R^2 of 100 PLSR models per training proportion are represented.
(DOCX)

Acknowledgments

The authors thank Kyle D. Morton for assistance in the field. We also thank John Adams and Ian M. Shiach for maintaining the poplar plantation.

Author Contributions

Conceptualization: Mallory L. Barnes, David D. Breshears, Darin J. Law, David J. P. Moore.

Data curation: Mallory L. Barnes, Alec C. Fojtik.

Formal analysis: Mallory L. Barnes, Greg A. Barron-Gafford.

Funding acquisition: David J. P. Moore.

Investigation: Mallory L. Barnes, Darin J. Law, Willem J. D. van Leeuwen, Alec C. Fojtik, Greg A. Barron-Gafford, David J. P. Moore.

Methodology: Mallory L. Barnes, Darin J. Law, Willem J. D. van Leeuwen, Alec C. Fojtik, David J. P. Moore.

Project administration: David D. Breshears, Darin J. Law, Russell K. Monson, Greg A. Barron-Gafford, David J. P. Moore.

Resources: David D. Breshears, Willem J. D. van Leeuwen, Russell K. Monson, David J. P. Moore.

Software: Willem J. D. van Leeuwen.

Supervision: David D. Breshears, Russell K. Monson, David J. P. Moore.

Validation: Mallory L. Barnes, Russell K. Monson.

Visualization: Mallory L. Barnes.

Writing – original draft: Mallory L. Barnes.

Writing – review & editing: David D. Breshears, Darin J. Law, Willem J. D. van Leeuwen, Russell K. Monson, Alec C. Fojtik, Greg A. Barron-Gafford, David J. P. Moore.

References

1. Foley JA, Prentice IC, Ramankutty N, Levis S, Pollard D, Sitch S, et al. An integrated biosphere model of land surface processes, terrestrial carbon balance, and vegetation dynamics. Glob Biogeochem Cycles. 1996; 10: 603–628. https://doi.org/10.1029/96GB02692
2. Zaehle S, Friend AD. Carbon and nitrogen cycle dynamics in the O-CN land surface model: 1. Model description, site-scale evaluation, and sensitivity to parameter estimates. Glob Biogeochem Cycles. 2010; 24: GB1005. https://doi.org/10.1029/2009GB003521
3. Bonan GB, Lawrence PJ, Oleson KW, Levis S, Jung M, Reichstein M, et al. Improving canopy processes in the Community Land Model version 4 (CLM4) using global flux fields empirically inferred from

FLUXNET data. J Geophys Res Biogeosciences. 2011; 116: G02014. https://doi.org/10.1029/2010JG001593

4. Quéré CL, Moriarty R, Andrew RM, Canadell JG, Sitch S, Korsbakken JI, et al. Global Carbon Budget 2015. Earth Syst Sci Data. 2015; 7: 349–396. https://doi.org/10.5194/essd-7-349-2015
5. Cao M, Woodward FI. Dynamic responses of terrestrial ecosystem carbon cycling to global climate change. Nature. 1998; 393: 249–252. https://doi.org/10.1038/30460
6. Schimel D, Melillo J, Tian H, McGuire AD, Kicklighter D, Kittel T, et al. Contribution of Increasing CO2 and Climate to Carbon Storage by Ecosystems in the United States. Science. 2000; 287: 2004–2006. https://doi.org/10.1126/science.287.5460.2004 PMID: 10720324
7. Frank D, Reichstein M, Bahn M, Thonicke K, Frank D, Mahecha MD, et al. Effects of climate extremes on the terrestrial carbon cycle: concepts, processes and potential future impacts. Glob Change Biol. 2015; 21: 2861–2880. https://doi.org/10.1111/gcb.12916 PMID: 25752680
8. Xia J, Chen J, Piao S, Ciais P, Luo Y, Wan S. Terrestrial carbon cycle affected by non-uniform climate warming. Nat Geosci. 2014; 7: 173–180. https://doi.org/10.1038/ngeo2093
9. Beer C, Reichstein M, Tomelleri E, Ciais P, Jung M, Carvalhais N, et al. Terrestrial Gross Carbon Dioxide Uptake: Global Distribution and Covariation with Climate. Science. 2010; 329: 834–838. https://doi.org/10.1126/science.1184984 PMID: 20603496
10. Nijp JJ, Limpens J, Metselaar K, van der Zee SEATM, Berendse F, Robroek BJM. Can frequent precipitation moderate the impact of drought on peatmoss carbon uptake in northern peatlands? New Phytol. 2014; 203: 70–80. https://doi.org/10.1111/nph.12792 PMID: 24689361
11. Reich PB, Hobbie SE, Lee TD. Plant growth enhancement by elevated CO2 eliminated by joint water and nitrogen limitation. Nat Geosci. 2014; 7: 920–924. https://doi.org/10.1038/ngeo2284
12. Keenan TF, Hollinger DY, Bohrer G, Dragoni D, Munger JW, Schmid HP, et al. Increase in forest water-use efficiency as atmospheric carbon dioxide concentrations rise. Nature. 2013; 499: 324–327. https://doi.org/10.1038/nature12291 PMID: 23842499
13. Morecroft MD, Stokes VJ, Morison JIL. Seasonal changes in the photosynthetic capacity of canopy oak (Quercus robur) leaves: the impact of slow development on annual carbon uptake. Int J Biometeorol. 2003; 47: 221–226. https://doi.org/10.1007/s00484-003-0173-3 PMID: 12733054
14. Friedlingstein P, Meinshausen M, Arora VK, Jones CD, Anav A, Liddicoat SK, et al. Uncertainties in CMIP5 Climate Projections due to Carbon Cycle Feedbacks. J Clim. 2013; 27: 511–526. https://doi.org/10.1175/JCLI-D-12-00579.1
15. Running SW, Nemani RR. Relating seasonal patterns of the AVHRR vegetation index to simulated photosynthesis and transpiration of forests in different climates. Remote Sens Environ. 1988; 24: 347–367. https://doi.org/10.1016/0034-4257(88)90034-X
16. Zhou L, Tucker CJ, Kaufmann RK, Slayback D, Shabanov NV, Myneni RB. Variations in northern vegetation activity inferred from satellite data of vegetation index during 1981 to 1999. J Geophys Res Atmospheres. 2001; 106: 20069–20083. https://doi.org/10.1029/2000JD000115
17. Barnes ML, Moran MS, Scott RL, Kolb TE, Ponce-Campos GE, Moore DJP, et al. Vegetation productivity responds to sub-annual climate conditions across semiarid biomes. Ecosphere. 2016; 7: n/a-n/a. https://doi.org/10.1002/ecs2.1339
18. Shi H, Li L, Eamus D, Huete A, Cleverly J, Tian X, et al. Assessing the ability of MODIS EVI to estimate terrestrial ecosystem gross primary production of multiple land cover types. Ecol Indic. 2017; 72: 153–164. https://doi.org/10.1016/j.ecolind.2016.08.022
19. Running SW, Nemani RR, Heinsch FA, Zhao M, Reeves M, Hashimoto H. A Continuous Satellite-Derived Measure of Global Terrestrial Primary Production. BioScience. 2004; 54: 547–560. https://doi.org/10.1641/0006-3568(2004)054[0547:ACSMOG]2.0.CO;2
20. Asrar G, Fuchs M, Kanemasu ET, Hatfield JL. Estimating Absorbed Photosynthetic Radiation and Leaf Area Index from Spectral Reflectance in Wheat. Agron J. 1984; 76: 300–306. https://doi.org/10.2134/agronj1984.00021962007600020029x
21. Fensholt R, Sandholt I, Rasmussen MS. Evaluation of MODIS LAI, fAPAR and the relation between fAPAR and NDVI in a semi-arid environment using in situ measurements. Remote Sens Environ. 2004; 91: 490–507. https://doi.org/10.1016/j.rse.2004.04.009
22. Huete A, Ponce-Campos G, Zhang Y, Restrepo-Coupe N, Ma X, Moran MS. Monitoring Photosynthesis from Space [Internet]. CRC Press; 2016. Available: https://opus.lib.uts.edu.au/handle/10453/73083
23. Ruimy A, Jarvis PG, Baldocchi DD, Saugier B. CO2 Fluxes over Plant Canopies and Solar Radiation: A Review. Adv Ecol Res. 1995; 26: 1–68. https://doi.org/10.1016/S0065-2504(08)60063-X
24. Turner DP, Urbanski S, Bremer D, Wofsy SC, Meyers T, Gower ST, et al. A cross-biome comparison of daily light use efficiency for gross primary production. Glob Change Biol. 2003; 9: 383–395. https://doi.org/10.1046/j.1365-2486.2003.00573.x

25. Sims DA, Rahman AF, Cordova VD, El-Masri BZ, Baldocchi DD, Flanagan LB, et al. On the use of MODIS EVI to assess gross primary productivity of North American ecosystems. J Geophys Res Biogeosciences. 2006; 111: G04015. https://doi.org/10.1029/2006JG000162

26. Jenkins JP, Richardson AD, Braswell BH, Ollinger SV, Hollinger DY, Smith M-L. Refining light-use efficiency calculations for a deciduous forest canopy using simultaneous tower-based carbon flux and radiometric measurements. Agric For Meteorol. 2007; 143: 64–79. https://doi.org/10.1016/j.agrformet.2006.11.008

27. Rogers A. The use and misuse of Vc,max in Earth System Models. Photosynth Res. 2014; 119: 15–29. https://doi.org/10.1007/s11120-013-9818-1 PMID: 23564478

28. Verbeeck H, Peylin P, Bacour C, Bonal D, Steppe K, Ciais P. Seasonal patterns of CO2 fluxes in Amazon forests: Fusion of eddy covariance data and the ORCHIDEE model. J Geophys Res Biogeosciences. 2011; 116: G02018. https://doi.org/10.1029/2010JG001544

29. Gitelson AA, Gamon JA, Solovchenko A. Multiple drivers of seasonal change in PRI: Implications for photosynthesis 1. Leaf level. Remote Sens Environ. 2017; 191: 110–116. https://doi.org/10.1016/j.rse.2016.12.014

30. Gamon JA, Peñuelas J, Field CB. A narrow-waveband spectral index that tracks diurnal changes in photosynthetic efficiency. Remote Sens Environ. 1992; 41: 35–44. https://doi.org/10.1016/0034-4257(92)90059-S

31. Farquhar GD, Caemmerer S von, Berry JA. A biochemical model of photosynthetic CO2 assimilation in leaves of C3 species. Planta. 149: 78–90. https://doi.org/10.1007/BF00386231 PMID: 24306196

32. Serbin SP, Dillaway DN, Kruger EL, Townsend PA. Leaf optical properties reflect variation in photosynthetic metabolism and its sensitivity to temperature. J Exp Bot. 2012; 63: 489–502. https://doi.org/10.1093/jxb/err294 PMID: 21984647

33. Serbin SP, Singh A, Desai AR, Dubois SG, Jablonski AD, Kingdon CC, et al. Remotely estimating photosynthetic capacity, and its response to temperature, in vegetation canopies using imaging spectroscopy. Remote Sens Environ. 2015; 167: 78–87. https://doi.org/10.1016/j.rse.2015.05.024

34. Kattge J, Knorr W. Temperature acclimation in a biochemical model of photosynthesis: a reanalysis of data from 36 species. Plant Cell Environ. 2007; 30: 1176–1190. https://doi.org/10.1111/j.1365-3040.2007.01690.x PMID: 17661754

35. Dreyer E, Le Roux X, Montpied P, Daudet FA, Masson F. Temperature response of leaf photosynthetic capacity in seedlings from seven temperate tree species. Tree Physiol. 2001; 21: 223–232. https://doi.org/10.1093/treephys/21.4.223 PMID: 11276416

36. Bernacchi CJ, Calfapietra C, Davey PA, Wittig VE, Scarascia-Mugnozza GE, Raines CA, et al. Photosynthesis and stomatal conductance responses of poplars to free-air CO2 enrichment (PopFACE) during the first growth cycle and immediately following coppice. New Phytol. 2003; 159: 609–621. https://doi.org/10.1046/j.1469-8137.2003.00850.x

37. Limousin J-M, Misson L, Lavoir A-V, Martin NK, Rambal S. Do photosynthetic limitations of evergreen Quercus ilex leaves change with long-term increased drought severity? Plant Cell Environ. 2010; 33: 863–875. https://doi.org/10.1111/j.1365-3040.2009.02112.x PMID: 20051039

38. Onoda Y, Hikosaka K, Hirose T. The balance between RuBP carboxylation and RuBP regeneration: a mechanism underlying the interspecific variation in acclimation of photosynthesis to seasonal change in temperature. Funct Plant Biol. 2005; 32: 903–910. https://doi.org/10.1071/FP05024

39. Xu L, Baldocchi DD. Seasonal trends in photosynthetic parameters and stomatal conductance of blue oak (Quercus douglasii) under prolonged summer drought and high temperature. Tree Physiol. 2003; 23: 865–877. https://doi.org/10.1093/treephys/23.13.865 PMID: 14532010

40. Wilson KB, Baldocchi DD, Hanson PJ. Spatial and seasonal variability of photosynthetic parameters and their relationship to leaf nitrogen in a deciduous forest. Tree Physiol. 2000; 20: 565–578. https://doi.org/10.1093/treephys/20.9.565 PMID: 12651421

41. Ainsworth EA, Serbin SP, Skoneczka JA, Townsend PA. Using leaf optical properties to detect ozone effects on foliar biochemistry. Photosynth Res. 2014; 119: 65–76. https://doi.org/10.1007/s11120-013-9837-y PMID: 23657827

42. Yendrek C, Tomaz T, Montes CM, Cao Y, Morse AM, Brown PJ, et al. High-throughput phenotyping of maize leaf physiology and biochemistry using hyperspectral reflectance. Plant Physiol. 2016; pp.01447.2016. https://doi.org/10.1104/pp.16.01447 PMID: 28049858

43. Heckmann D, Schlüter U, Weber APM. Machine Learning Techniques for Predicting Crop Photosynthetic Capacity from Leaf Reflectance Spectra. Mol Plant. 2017; 10: 878–890. https://doi.org/10.1016/j.molp.2017.04.009 PMID: 28461269

44. Sims DA, Gamon JA. Relationships between leaf pigment content and spectral reflectance across a wide range of species, leaf structures and developmental stages. Remote Sens Environ. 2002; 81: 337–354. https://doi.org/10.1016/S0034-4257(02)00010-X

45. Smith M-L, Ollinger SV, Martin ME, Aber JD, Hallett RA, Goodale CL. Direct Estimation of Aboveground Forest Productivity Through Hyperspectral Remote Sensing of Canopy Nitrogen. Ecol Appl. 2002; 12: 1286–1302. https://doi.org/10.1890/1051-0761(2002)012[1286:DEOAFP]2.0.CO;2

46. Rahman AF, Gamon JA, Fuentes DA, Roberts DA, Prentiss D. Modeling spatially distributed ecosystem flux of boreal forest using hyperspectral indices from AVIRIS imagery. J Geophys Res Atmospheres. 2001; 106: 33579–33591. https://doi.org/10.1029/2001JD900157

47. Stimson HC, Breshears DD, Ustin SL, Kefauver SC. Spectral sensing of foliar water conditions in two co-occurring conifer species: Pinus edulis and Juniperus monosperma. Remote Sens Environ. 2005; 96: 108–118. https://doi.org/10.1016/j.rse.2004.12.007

48. Duursma RA. Plantecophys—An R Package for Analysing and Modelling Leaf Gas Exchange Data. Struik PC, editor. PLOS ONE. 2015; 10: e0143346. https://doi.org/10.1371/journal.pone.0143346 PMID: 26581080

49. Wehrens R, Mevik B-H. The pls Package: Principal Component and Partial Least Squares Regression in R. 24. 2007; Available: http://repository.ubn.ru.nl/handle/2066/36604

50. Siegmann B, Jarmer T. Comparison of different regression models and validation techniques for the assessment of wheat leaf area index from hyperspectral data. Int J Remote Sens. 2015; 36: 4519–4534. https://doi.org/10.1080/01431161.2015.1084438

51. Farrés M, Platikanov S, Tsakovski S, Tauler R. Comparison of the variable importance in projection (VIP) and of the selectivity ratio (SR) methods for variable selection and interpretation: Comparison of variable selection methods. J Chemom. 2015; 29: 528–536. https://doi.org/10.1002/cem.2736

52. Gamon JA, Serrano L, Surfus JS. The photochemical reflectance index: an optical indicator of photosynthetic radiation use efficiency across species, functional types, and nutrient levels. Oecologia. 1997; 112: 492–501. https://doi.org/10.1007/s004420050337 PMID: 28307626

53. Drolet GG, Middleton EM, Huemmrich KF, Hall FG, Amiro BD, Barr AG, et al. Regional mapping of gross light-use efficiency using MODIS spectral indices. Remote Sens Environ. 2008; 112: 3064–3078. https://doi.org/10.1016/j.rse.2008.03.002

54. Gray SB, Dermody O, DeLucia EH. Spectral reflectance from a soybean canopy exposed to elevated CO2 and O3. J Exp Bot. 2010; 61: 4413–4422. https://doi.org/10.1093/jxb/erq244 PMID: 20696654

55. Dobrowski SZ, Pushnik JC, Zarco-Tejada PJ, Ustin SL. Simple reflectance indices track heat and water stress-induced changes in steady-state chlorophyll fluorescence at the canopy scale. Remote Sens Environ. 2005; 97: 403–414. https://doi.org/10.1016/j.rse.2005.05.006

56. Maia R, Eliason CM, Bitton P-P, Doucet SM, Shawkey MD. pavo: an R package for the analysis, visualization and organization of spectral data. Methods Ecol Evol. 2013; 4: 906–913. https://doi.org/10.1111/2041-210X.12069

57. Gitelson AA, Merzlyak MN. Remote estimation of chlorophyll content in higher plant leaves. Int J Remote Sens. 1997; 18: 2691–2697. https://doi.org/10.1080/014311697217558

58. le Maire G, François C, Dufrêne E. Towards universal broad leaf chlorophyll indices using PROSPECT simulated database and hyperspectral reflectance measurements. Remote Sens Environ. 2004; 89: 1–28. https://doi.org/10.1016/j.rse.2003.09.004

59. Vogelmann JE, Rock BN, Moss DM. Red edge spectral measurements from sugar maple leaves. Int J Remote Sens. 1993; 14: 1563–1575. https://doi.org/10.1080/01431169308953986

60. Carter GA. Ratios of leaf reflectances in narrow wavebands as indicators of plant stress. Int J Remote Sens. 1994; 15: 697–703. https://doi.org/10.1080/01431169408954109

61. Maccioni A, Agati G, Mazzinghi P. New vegetation indices for remote measurement of chlorophylls based on leaf directional reflectance spectra. J Photochem Photobiol B. 2001; 61: 52–61. https://doi.org/10.1016/S1011-1344(01)00145-2 PMID: 11485848

62. Gitelson AA, Buschmann C, Lichtenthaler HK. The Chlorophyll Fluorescence Ratio F735/F700 as an Accurate Measure of the Chlorophyll Content in Plants. Remote Sens Environ. 1999; 69: 296–302. https://doi.org/10.1016/S0034-4257(99)00023-1

63. Datt B. Remote Sensing of Chlorophyll a, Chlorophyll b, Chlorophyll a+b, and Total Carotenoid Content in Eucalyptus Leaves. Remote Sens Environ. 1998; 66: 111–121. https://doi.org/10.1016/S0034-4257(98)00046-7

64. Gao B. NDWI—A normalized difference water index for remote sensing of vegetation liquid water from space. Remote Sens Environ. 1996; 58: 257–266. https://doi.org/10.1016/S0034-4257(96)00067-3

65. Penuelas J. "Semi-empirical indices." Photosynthetica 31.2 (1995): 221–230. APA.

66. Doughty CE, Asner GP, Martin RE. Predicting tropical plant physiology from leaf and canopy spectroscopy. Oecologia. 2011; 165: 289–299. https://doi.org/10.1007/s00442-010-1800-4 PMID: 20963611

67. Hansen PM, Schjoerring JK. Reflectance measurement of canopy biomass and nitrogen status in wheat crops using normalized difference vegetation indices and partial least squares regression. Remote Sens Environ. 2003; 86: 542–553. https://doi.org/10.1016/S0034-4257(03)00131-7

68. Evans JR. Photosynthesis and nitrogen relationships in leaves of C3 plants. Oecologia. 1989; 78: 9–19. https://doi.org/10.1007/BF00377192 PMID: 28311896

69. Rogers A, Medlyn BE, Dukes JS, Bonan G, von Caemmerer S, Dietze MC, et al. A roadmap for improving the representation of photosynthesis in Earth system models. New Phytol. 2017; 213: 22–42. https://doi.org/10.1111/nph.14283 PMID: 27891647

70. Zaehle S, Sitch S, Smith B, Hatterman F. Effects of parameter uncertainties on the modeling of terrestrial biosphere dynamics. Glob Biogeochem Cycles. 2005; 19: GB3020. https://doi.org/10.1029/2004GB002395

71. Verheijen LM, Brovkin V, Aerts R, Bönish G, Cornelissen JHC, Kattge J, et al. Impacts of trait variation through observed trait-climate relationships on performance of a representative Earth System Model: a conceptual analysis. Biogeosciences. 2013; 10: 5497–5515. https://doi.org/10.5194/bg-10-5497-2013

72. Schimel D, Pavlick R, Fisher JB, Asner GP, Saatchi S, Townsend P, et al. Observing terrestrial ecosystems and the carbon cycle from space. Glob Change Biol. 2015; n/a-n/a. https://doi.org/10.1111/gcb.12822 PMID: 25472464

73. Walker AP, Beckerman AP, Gu L, Kattge J, Cernusak LA, Domingues TF, et al. The relationship of leaf photosynthetic traits–Vcmax and Jmax–to leaf nitrogen, leaf phosphorus, and specific leaf area: a meta-analysis and modeling study. Ecol Evol. 2014; 4: 3218–3235. https://doi.org/10.1002/ece3.1173 PMID: 25473475

74. Kampe TU, Johnson BR, Kuester M, Keller M. NEON: the first continental-scale ecological observatory with airborne remote sensing of vegetation canopy biochemistry and structure. J Appl Remote Sens. 2010; 4: 043510-043510-24. https://doi.org/10.1117/1.3501124

75. Lee CM, Cable ML, Hook SJ, Green RO, Ustin SL, Mandl DJ, et al. An introduction to the NASA Hyperspectral InfraRed Imager (HyspIRI) mission and preparatory activities. Remote Sens Environ. 2015; 167: 6–19. https://doi.org/10.1016/j.rse.2015.06.012